Journal of Magnetism and Magnetic Materials 504 (2020) 166659

Contents lists available at ScienceDirect

Journal of Magnetism and Magnetic Materials

journal homepage: www.elsevier.com/locate/jmmm

Research articles

The influence of residual stress on flux-barriers of non-oriented electrical steel

B. Schauerte[a,*], N. Leuning[a], S. Vogt[b], I. Moll[b], H. Weiss[b], T. Neuwirth[c], M. Schulz[c], W. Volk[b], K. Hameyer[a]

[a] Institute of Electrical Machines (IEM), RWTH Aachen University, Aachen, Germany
[b] Chair of Metal Forming and Casting (utg), TU Munich, Garching, Germany
[c] Heinz Maier-Leibnitz Zentrum (MLZ), TU Munich, Garching, Germany

A B S T R A C T

In rotating electrical machines, cutouts in the rotor laminations control the magnetic flux density distribution in the d- and q-axis of the magnetic core. Guiding the magnetic flux by cutouts leads to very narrow bridges in the electrical steel. However, at the same time, this can limit the maximum speed of a rotor e.g. due to the material's maximum allowed mechanical stress. Therefore, the centrifugal forces confine the achievable power density. The aim of this study is the examination of the effect of flux-barriers fabricated by mechanical embossing on the magnetic properties of non-oriented electrical steel. The embossing process causes a static residual stress distribution and thereby a reduction of the permeability resulting from *Villari*'s effect. The non-oriented electrical steel samples are embossed with varying distances between the barriers and measured at different angles to the barrier edges on a single-sheet tester. A comparison with respect to their directional and embossing geometry-dependent effectiveness as magnetic flux barriers is carried out. A correlation of the results with measurements of the local flux density, obtained by neutron-grating interferometry, is performed in order to enable a consideration of the mechanical embossing on the local magnetic flux density distribution.

1. Introduction

In experiments on the cut-edge effect [1–3] and the influence of mechanical stress [4,5], primarily the negative effects of residual stress on the magnetic material behavior of non-oriented electrical steel sheets have been analyzed. The Finite Element (FE) modeling of these influences has been the subject of research for many years and shows good agreement with measurements [6–10]. In addition to the negative consequences of dynamic and static residual stress on the magnetic behavior of the soft-magnetic core, the magneto-elastic coupling can be used for a targeted control and guidance of the magnetic flux density distribution. A suppression of stray flux can be achieved. One possible application of statically induced residual stress introduced to the sheet metal cross sectional area of the magnetic circuit, is the substitution of the commonly used cutouts in the magnetic core design of the permanent magnet positioning of permanent magnet synchronous machine (PMSM) rotors to reduce leakage flux.

The use of residual stress-based flux barriers, in addition to suppressing stray flux while increasing achievable rotational speeds, can also provide improved torque adjustment by a more targeted control of the magnetic flux in the magnetically conductive d- and the flux oppressing q-axis.

For this purpose, embossings can be used to examine the residual stress in its effects on the material behavior at a global, as well on a local scale to allow estimations regarding their applicability by magneto-mechanical simulations. In order to be able to transfer the existing insights and modeling approaches of the magneto-elastic coupling to FE simulations, high resolution knowledge about the residual stress distribution in industrially deformed electrical steel sheets is required. Furthermore, measurements of the global magnetic behavior are needed for the validation of the electromechanically coupled simulations. To localize the residual-stress introduced in the soft magnetic material by embossing, a new measuring method, neutron grating interferometry, was used. This technique allows to resolve the local magnetic domain wall density, which is influenced by the mechanical stress distribution and the applied magnetic field. Initial investigations into the electromagnetic efficiency by embossings of induced residual stress and its metrological quantifications have already been performed and are presented in [11]. Here, the decrease of the permeability can be attributed to the statically impressed residual stress. The geometric deformation of the sample takes a subordinate role.

* Corresponding author.
E-mail address: benedikt.schauerte@iem.rwth-aachen.de (B. Schauerte).

https://doi.org/10.1016/j.jmmm.2020.166659
Received 6 September 2019; Received in revised form 20 February 2020; Accepted 24 February 2020
Available online 28 February 2020
0304-8853/ © 2020 Elsevier B.V. All rights reserved.

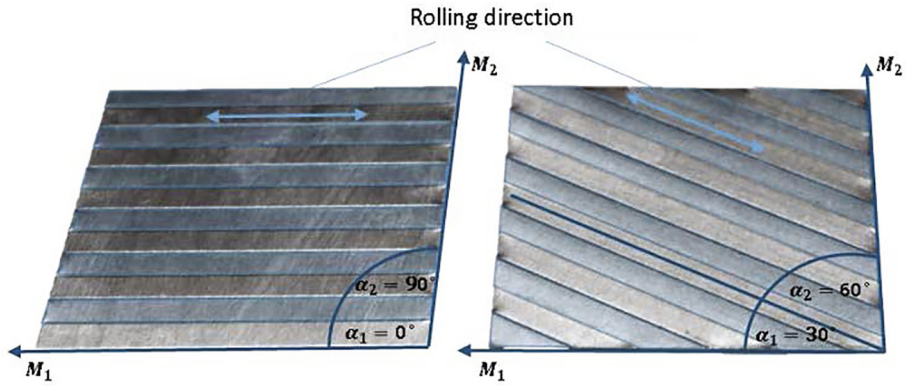

Fig. 1. Embossed samples for 0° and 90° measurements (left) and 30° and 60° to the rolling direction (right). Both depicted samples have a distance of 5 mm between embossing edges.

2. Methodology

For this work, 60 × 60 mm samples with a thickness of 0.5 mm and a Silicon content of 2.4 wt% were fabricated with embossing edges arranged parallel to the rolling direction (RD) and magnetically measured at different angles relative to the RD using a single-sheet-tester (SST). In analogy to cutting edge tests, the distance between the 5 mm wide embossing edges is varied in order to study the influence of the embossing density on the global magnetic properties. The distances δ_{dist} of unworked material between the embossing edges are chosen to be 5, 10 and 15 mm. The samples exemplarily depicted in Fig. 1 are measured at angles θ of 0, 30, 45, 60 and 90° between the direction of magnetization and the embossing edge, i.e., RD. The peak flux densitiy varying from 0.1 to 1.8 T is measured at magnetization frequencies of 50, 100 and 400 Hz respectively. Since the focus of the flux barriers is primarily on the magnetizability of the material, the permeability with respect to the actual magnetic polarization is the decisive criterion. The reversal points of the increasing hysteresis curves are used as support points to calculate the relative permeability.

Next to the magnetizability of the material, the occurring iron losses are of particular interest, as they do not occur in the commonly used flux barriers formed by the cutouts in the magnetic core. For the comparison of the occurring losses with respect to the different angles between flux barriers respective embossing edges and the magnetization direction, measurements at 100 Hz will be compared for each embossing distance δ_{dist}. Due to the sample geometry, a certain distortion of the measurement results must be expected. In contrast to conventional flat-surface samples, only approximately half of the total area of the embossed samples close the magnetic circuit of the double yoke SST. This could lead to the consequence that the magnetic resistance of the yokes of the SST is no longer completely negligible and thus influences the measurements. In addition to the magnetic measurements performed on the SST, which provide insight into the globally averaged directional dependence of the flux barriers, neutron grating interferometry (nGI) measurements were performed, providing information about the local magnetic domain wall density.

In contrast to standard neutron imaging, nGI does not only depend on the attenuation of neutrons passing through the sample, but also delivers information about the ultra-small-angle scattering of neutrons (USANS) caused by material inhomogeneity and magnetic domain structures. By analyzing the scattering, the local magnetic domain structure can be mapped in the dark-field image (DFI). Especially, when using grain-oriented electrical tapes this technique has shown that in-situ investigations of the domain structure under different stress states, field amplitudes and field frequencies can be performed [12,13]. Due to the large magnetic domains in grain-oriented electrical tapes, a direct visualization of the magnetic domain walls has been achieved. In contrast the magnetic domains of non-grain-oriented electrical steel tapes are below the spatial resolution of the detector (roughly 100 µm), hence the DFI maps the density of domain walls in an area in contrast to imaging examination technologies as presented in [14]. In [15] it is shown that this information is related to the residual stress in the sample, allowing to directly quantify the range of the perturbation of the magnetic structure at a cutting edge.

3. Results and discussion

The measurements depicted in Fig. 2 show the influence of the distance between the embossing edges on the relative permeability μ_r of the material as a function of the respective peak polarization J_m at different angles to the cutting edge and therefore the RD of the samples (b–d). For comparison, an anisotropy measurement of the same material without residual stress is depicted in Fig. 2a). The measurement in RD with a maximum relative permeability of almost 12,000 is by far superior in terms of magnetizability. While the permeability of the material decreases with an increasing angle θ between the direction of the magnetic field properties and RD until it is reduced to less than 50% in the transverse direction (TD). The anisotropy of the unworked material is mostly pronounced for polarizations between 0.5 and 1.0 T, while the measured curves converge to a common value at higher polarizations up to 1.8 T. This general trend of a high relative permeability for the measurement at 0° and decreasing magnetizabilities with increasing misalignments between the direction of the magnetic measurement and the RD is also visible for the samples with residual stress. In comparison to the original anisotropy measurement without embossing edges, the permeability generally decreases for increasing angles θ and decreasing edge distances δ_{dist}. The measurements obtained for samples with a distance δ_{dist} of 15 mm between the embossing edges still reveals considerable differences in terms of the magnetizability. The measurement performed at $\theta = 0°$ has the highest relative permeability for each evaluated distance between the embossings δ_{dist}. Also, the density of the embossings has the highest influence on the samples measured at 0°. Regarding the 90°-measurement the permeability is already strongly decreased for embossing edges with a distance of 15 mm. Although, permeability is also reduced for this angle by an increasing number of embossings, the embossings are already at a distance of 15 mm electromagnetically effective barriers for the magnetic flux. The measured curves approximate more and more for decreasing distances δ_{dist}, as the residual stress concentration in the non-embossed areas increases with increasing number of embossing edges. In addition to this approximation of the absolute permeability values with decreasing δ_{dist} for all peak flux densities B_m, the behavior of the various angle samples is becoming increasingly inhomogeneous. While the relative permeability of the unprocessed and the embossed sample with an edge distance of 15 mm decreases for all peak flux densities, the material behavior is less clear for the denser

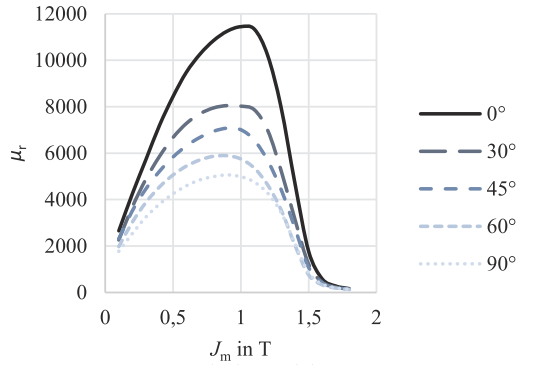

a) Unworked material.

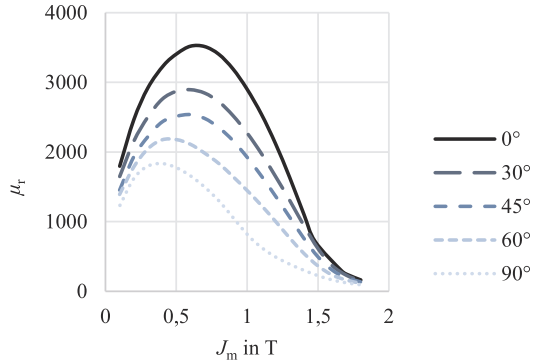

b) Embossing distance δ_{dist} = 15 mm.

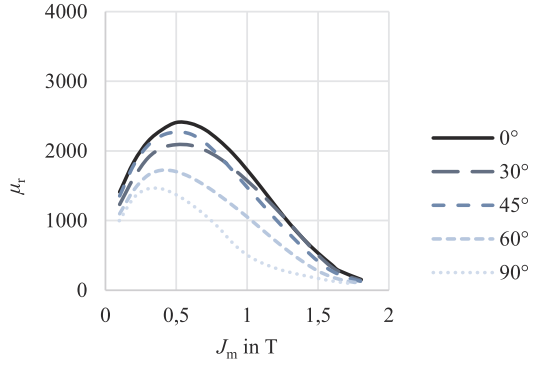

c) Embossing distance δ_{dist} = 10 mm.

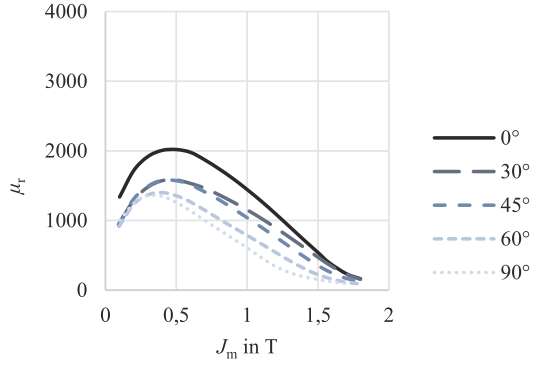

d) Embossing distance δ_{dist} = 5 mm.

Fig. 2. Relative permeability of unworked material a) and samples with different distances δ_{dist} between embossing edges b)–d) measured at 100 Hz at different angles to RD.

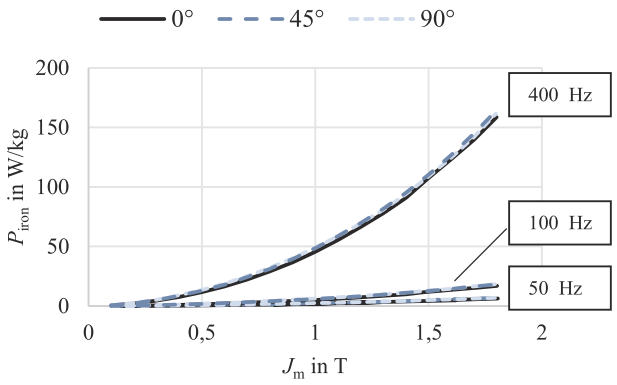

a) Embossing distance δ_{dist} = 15 mm.

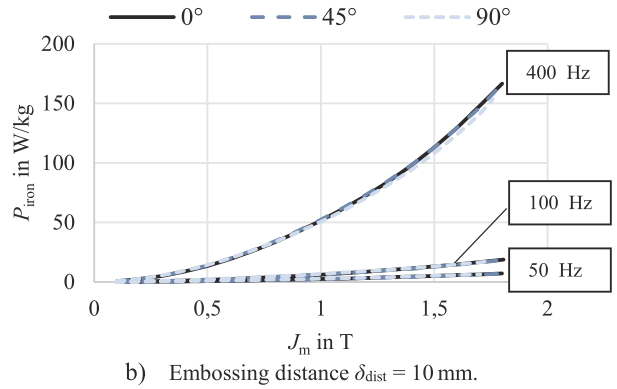

b) Embossing distance δ_{dist} = 10 mm.

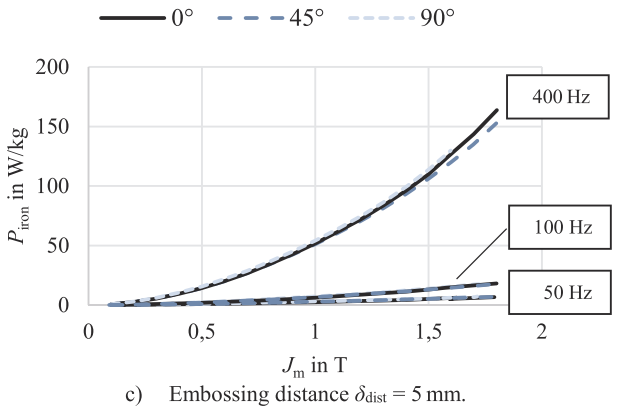

c) Embossing distance δ_{dist} = 5 mm.

Fig. 3. Resulting iron loss P_{iron} with respect of peak polarizations J_m for different δ_{dist} for magnetization frequencies of 50, 100 and 400 Hz with angles of 0°, 45° and 90° between magnetization direction of cutting edges, respective RD.

punched samples. The unembossed areas can be interpreted as the magnetic conductive axes, respective the d-axis in analogy to electrical machines. For these axes, arranged parallel to the embossing edges, too strong influences evoked by the introduced residual stress are not desirable. Regarding the measurements performed on the samples with the embossings distances of 10 and 5 mm depicted in Fig. 2 c) and d) it is notable, that the magnetizability of the RD sample is least distinctive for the samples with δ_{dist} of 10 mm. It can also be observed that the peak value of the permeability shifts with increasing embossing densities towards lower polarizations. For the 90° measurement this is already the case for an embossing distance of 15 mm. The other angles follow successively, until the permeability measured at 0° and 5 mm also has its maximum at 0.5 T. The cause of these effects has to be examined in deeper analysis including the locally resolved residual stress distribution as input for FE analysis linked with a magneto-mechanical anisotropy model.

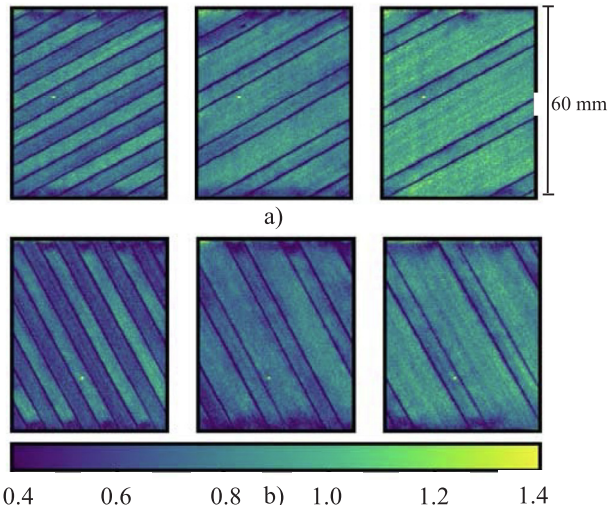

Fig. 4. Normalized signal of DFI-contrast at 30° (a) and 60° (b) between magnetization direction and embossing edges respective RD. The applied magnetic field strength is 780 °A/m. A signal below one denotes a reduced magnetic flux density due to residual stress.

In contrast to the magnetizability, which is strongly influenced by the embossings, the measurements of the resulting iron losses show no decisive dependence on the introduced residual stress. Fig. 3 shows the resulting losses of the three different embossing distances at 0, 45 and 90° between the magnetization direction and the embossing edges, or the RD. A clear correlation between the impressions and spatial directions as well as the measured iron losses can not be drawn. Measured by the deviations of the magnetic permeability, the differences between the iron losses can be neglected. This behavior is in contrast to measurements of non-oriented electrical steel under the influence of mechanical stress, respective cutting edge measurements. The nGI measurements confirm the observations from the magnetic measurements on the SST. Fig. 4 shows the results of the domain wall density measurements performed with the neutron grating interferometer at the instrument ANTARES [16,17] at FRM II and allows conclusions to be drawn about the local distribution of the magnetic flux density at different embossing distances of a 30° and 60° sample. The depicted measurements were performed at an applied magnetic field strength of 780 A/m. The signal values were normalized by nGI measurements of unworked samples. A signal smaller than one therefore displays a reduced magnetic flux density. A signal higher than one indicates a local concentration of the magnetic flux. Analog to the measurements performed on the SST, the DFI-contrasts of the samples with a distance of 15 mm between the embossings have the brightest proportions. In comparison to the 60° measurement, the 30°-DFI-contrasts reveal the higher local flux densities. For every angle θ and each δ_{dist}, the non-embossed areas of the samples reveal higher levels of magnetization, fulfilling their purpose as magnetic conducting bridges inside of the material.

4. Conclusions

In this work, magnetic flux barriers were fabricated by parallel plastic deformation at different angles to the magnetization direction in the non-oriented electrical steel samples. The samples were globally tested regarding their magnetizability on a double yoke 60 × 60 mm SST. A decrease of the magnetic permeability, which increases with the angle between magnetization direction and embossing edges is observed. While the samples with a distance of 15 mm between the embossing edges allow a clear distinction between magnetically conducting and blocking axis, this effect is reduced for shorter distances due to increasing mechanical residual stress in the non-embossed areas of the material. The results were validated by local nGI domain wall density measurements. Mechanical simulations of the residual stress distribution and their coupling with a magneto-mechanical anisotropy model are planned for the future in order to allow a clearer distinction between the magnetic conducting and the blocking axis and provide deeper insights on the inhomogeneous behavior for smaller distances between the embossing edges.

CRediT authorship contribution statement

B. Schauerte: Writing - original draft, Visualization, Methodology. **N. Leuning:** Supervision, Conceptualization. **S. Vogt:** Writing - review & editing. **I. Moll:** Writing - review & editing, Methodology. **H. Weiss:** Supervision. **T. Neuwirth:** Methodology, Visualization. **M. Schulz:** Supervision, Project administration, Writing - review & editing. **W. Volk:** Supervision, Project administration, Writing - review & editing. **K. Hameyer:** Supervision, Project administration, Writing - review & editing.

Declaration of Competing Interest

The authors declare that they have no known competing financial interests or personal relationships that could have appeared to influence the work reported in this paper.

Acknowledgments

This work was supported by the Deutsche Forschungsgemeinschaft (DFG) and performed in the frame of the DFG research group project–“FOR 1897–Low-Loss Electrical Steel for Energy-Efficient Electrical Drives” and in the DFG priority program–“SPP2013–Focused Local Stress Imprint in Electrical Steel as Means of Improving the Energy Efficiency” - HA 4395/22-1; SCHU 3227/2-1; VO 1487/31-1. The results of this work are based upon experiments performed at the ANTARES instrument at Heinz Maier-Leibnitz Zentrum (MLZ), Garching, Germany.

References

[1] R. Siebert, J. Schneider, E. Beyer, Laser cutting and mechanical cutting of electrical steels and its effect on the magnetic properties, IEEE Trans. Magn. 50 (4) (2014) 1–4.
[2] H.A. Weiss, N. Leuning, S. Steentjes, K. Hameyer, T. Andorfer, S. Jenner, W. Volk, Influence of shear cutting parameters on the electromagnetic properties of non-oriented electrical steel sheets, J. Magn. Magn. Mater. 421 (2017) 250–259.
[3] H. Naumoski, B. Riedmüller, A. Minkow, U. Herr, Investigation of the influence of different cutting procedures on the global and local magnetic properties of non-oriented electrical steel, J. Magn. Magn. Mater. 392 (2015) 126–133.
[4] N. Leuning, S. Steentjes, M. Schulte, W. Bleck, K. Hameyer, Effect of elastic and plastic tensile mechanical loading on the magnetic properties of NGO electrical steel, J. Magn. Magn. Mater. 417 (2016) 42–48.
[5] J. Karthaus, S. Steentjes, D. Gröbel, K. Andreas, M. Merklein, K. Hameyer, Influence of the mechanical fatigue progress on the magnetic properties of electrical steel sheets, Arch. Electr. Eng. 66 (2) (2017) 351–360.
[6] M. Hofmann, H. Naumoski, U. Herr, H.G. Herzog, Magnetic properties of electrical steel sheets in respect of cutting: micromagnetic analysis and macromagnetic modeling, IEEE Trans. Magn. 52 (2) (2015) 1–14.
[7] M. Bali, H. De Gersem, A. Muetze, Finite-element modeling of magnetic material degradation due to punching, IEEE Trans. Magn. 50 (2) (2014) 745–748.
[8] S. Steentjes, G. von Pfingsten, K. Hameyer, An application-oriented approach for consideration of material degradation effects due to cutting on iron losses and magnetizability, IEEE Trans. Magn. 50 (11) (2014) 1–4.
[9] A. Belahcen, D. Singh, P. Rasilo, F. Martin, S.G. Ghalamestani, L. Vandevelde, Anisotropic and strain-dependent model of magnetostriction in electrical steel sheets, IEEE Trans. Magn. 51 (3) (2015) 1–4.
[10] L. Daniel, An analytical model for the effect of multiaxial stress on the magnetic susceptibility of ferromagnetic materials, IEEE Trans. Magn. 49 (5) (2013) 2037–2040.
[11] S. Vogt, T. Neuwirth, B. Schauerte, H.A. Weiss, P.M. Falger, A. Gustschin, W. Volk, Extent of embossing-related residual stress on the magnetic properties evaluated using neutron grating interferometry and single sheet test, Prod. Eng. 13 (2) (2019) 211–217.

[12] B. Betz, P. Rauscher, R.P. Harti, R. Schäfer, H. Van Swygenhoven, A. Kaestner, C. Grünzweig, Frequency-induced bulk magnetic domain-wall freezing visualized by neutron dark-field imaging, Phys. Rev. Appl. 6 (2) (2016) 024024.
[13] B. Betz, P. Rauscher, R.P. Harti, R. Schäfer, A. Irastorza-Landa, H. Van Swygenhoven, C. Grünzweig, Magnetization response of the bulk and supplementary magnetic domain structure in high-permeability steel laminations visualized in situ by neutron dark-field imaging, Phys. Rev. Appl. 6 (2) (2016) 024023.
[14] J. Liu, G.Y. Tian, B. Gao, K. Zeng, Y. Zheng, J. Chen, Micro-macro characteristics between domain wall motion and magnetic Barkhausen noise under tensile stress, J. Magn. Magn. Mater. 493 (2020) 165719.
[15] Siebert, R., Wetzig, A., Beyer, E., Betz, B., Grünzweig, C., & Lehmann, E. (2013, October). "Localized investigation of magnetic bulk property deterioration of electrical steel: Analysing magnetic property drop thorough mechanical and laser cutting of electrical steel laminations using neutron grating interferometry." In 2013 3rd International Electric Drives Production Conference (EDPC) (pp. 1-5). IEEE.
[16] M. Schulz, B. Schillinger, ANTARES: Cold neutron radiography and tomography facility, J. Large-Scale Res. Facil. JLSRF 1 (2015) 17.
[17] E. Calzada, F. Gruenauer, M. Mühlbauer, B. Schillinger, M. Schulz, New design for the ANTARES-II facility for neutron imaging at FRM II, Nucl. Instrum. Methods Phys. Res. Sect. A 605 (1–2) (2009) 50–53.